

Cronfa - Swansea University Open Access Repository

This is an author produced version of a paper published in :

Nanoscale

Cronfa URL for this paper:

<http://cronfa.swan.ac.uk/Record/cronfa21240>

Paper:

Lai, S., Luk, C., Tang, L., Teng, K. & Lau, S. (2015). Photoresponse of polyaniline-functionalized graphene quantum dots. *Nanoscale*, 7(12), 5338-5343.

<http://dx.doi.org/10.1039/c4nr07565j>

This article is brought to you by Swansea University. Any person downloading material is agreeing to abide by the terms of the repository licence. Authors are personally responsible for adhering to publisher restrictions or conditions. When uploading content they are required to comply with their publisher agreement and the SHERPA Romeo database to judge whether or not it is copyright safe to add this version of the paper to this repository.

<http://www.swansea.ac.uk/iss/researchsupport/cronfa-support/>

Cite this: DOI: 10.1039/c0xx00000x

www.rsc.org/xxxxxx

ARTICLE TYPE

Photoresponse of polyaniline-functionalized graphene quantum dots

Sin Ki Lai^a, Chi Man Luk^{a,b}, Libin Tang^{a,b}, Kar Seng Teng^c and Shu Ping Lau^{a,b*}

Received (in XXX, XXX) Xth XXXXXXXXX 20XX, Accepted Xth XXXXXXXXX 20XX

DOI: 10.1039/b000000x

5 Polyaniline-functionalized graphene quantum dots (PANI-GQD) and pristine graphene quantum dots (GQDs) were utilized for optoelectronic devices. PANI-GQD based photodetector exhibit higher responsivity which is about an order of magnitude at 405 nm and 7 folds at 532 nm as compared to GQD-based photodetector. The improved photoresponse is attributed to the enhanced interconnection of GQD by the island-like polymer matrices, which facilitates the carrier transport within the polymer matrices.
10 The optically tunable current-voltage (*I-V*) hysteresis of PANI-GQD is also demonstrated. The hysteresis magnifies progressively with light intensity at the scan range of ± 1 V. Both GQD and PANI-GQD devices change from positive to negative photocurrent when the bias reaches 4 V. Photogenerated carriers are excited to the trapping states in GQDs at increased bias. The trapped charges interact with charges injected from the electrodes which results in a net decrease of free charge carriers and a negative
15 photocurrent. The photocurrent switching phenomenon in GQD and PANI-GQD devices may open up novel applications in optoelectronics.

Introduction

Graphene quantum dots (GQDs) have attracted intense interest in the past few years as they exhibit strong photoluminescence (PL)¹⁻², coupled with other properties, such as heavy metal-free, bio-compatible³ and have good solubility in water, suitable for low cost fabrication. These advantages make GQDs very promising for use as fluorescent probes in bio-imaging.⁴⁻⁵ The outstanding optical property of GQDs has also drawn attention 20 for optoelectronic applications.⁶⁻¹² GQDs have been successfully utilized in light-emitting diodes^{6,10}, solar cells⁷⁻⁸ and photodetectors^{9,11-12}. Effective ways to synthesize GQDs with controllable properties are highly desirable for the above applications. Functionalization and making composites of GQDs 25 have shown to be an effective way to tailor the electrical and optical properties of GQDs.¹³⁻¹⁶ A number of works have been done on the amine-functionalization of GQDs. They demonstrated tunable PL peak position of the functionalized GQDs by varying the number of amine group on GQDs¹³ or by 30 varying the pH value to trigger the protonation of the alkyl amine group.¹⁶ Some works have also investigated the memory effect of P3HT-GQD¹⁷ and PEG-GQD¹⁸ composite by exploiting the hysteretic *I-V* relationship. The PEG-GQD composite¹⁹ and GQD-agar composite²⁰ were previously reported and their ability 35 in controlling the size of GQD and as phosphor for white light conversion were demonstrated respectively.
Recently, our group has synthesized GQD-polyaniline (PANI-GQD) nanocomposite.²¹ It has shown that the PL peak and hysteretic *I-V* behaviour of the PANI-GQD can be progressively 40 tuned by altering the amount of aniline in the synthesis process. In this work, we demonstrate that the hysteresis in PANI-GQD is

optically tunable. The optoelectronic properties of GQDs and PANI-GQD are also compared by studying their photoresponse. This study showed that PANI-GQD exhibits a higher responsivity 45 and shorter response time under visible light illumination. The responsivity of PANI-GQD device is an order of magnitude higher than GQD at 405 nm. Furthermore, both the GQD and PANI-GQD devices demonstrate a positive photocurrent at bias below 3 V, and change to a negative photocurrent when the bias 50 is above 4 V. Positive photocurrent can be reverted when voltage is reduced to below 3 V. Such switching behaviour has not been described in other GQD-based photodetectors. Its origin is discussed, and further investigation is needed for a better understanding of the switching behaviour. This voltage controlled 55 optical switching property may find novel application in optoelectronics.

Experimental

Synthesis of GQD

GQDs were synthesized by a microwave-assisted hydrothermal treatment of glucose solution. Glucose powder was dissolved in deionized (DI) water at 11 wt% and then sonicated for 15 min. The use of high wt% of glucose is to produce high concentration of GQDs. The solution was capped in a glass tube and heated by microwave for 5 min with the pressure controlled at 180 psi and 70 temperature at about 180°C. GQDs were formed during the microwave hydrothermal treatment. The solution was then centrifuged at 5000 rpm for 20 min and the GQD solution was obtained from the supernatant.

Synthesis of PANI-GQD

75 The aniline monomer of 2.5 mmol was added into the GQD

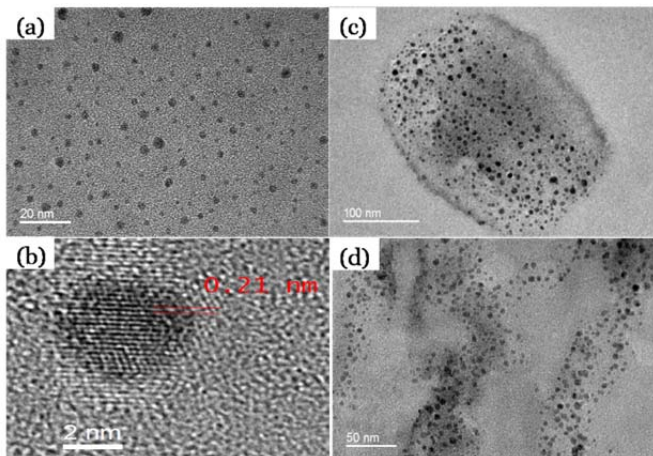


Figure 1 (a) TEM image of the GQDs. (b) HR-TEM image of the single GQD showing the lattice spacing of 0.21 nm. (c) and (d) TEM images of the PANI-GQD.

solution obtained above. Hydrochloric acid (HCl, 37%) was added drop-wise into the mixture to give 0.5 M HCl under continuous stirring. The mixture was sonicated for 15 min to allow uniform dispersion of aniline. It was then heated at 80 °C in a water bath for 30 min, and cooled in an ice bath. Subsequently, 0.1 M ammonium persulphate solution, acting as an oxidizing agent, was poured into the mixture and stirred thoroughly. The solution was kept at 4 °C for one day for polymerization, and was then centrifuged at 3000 rpm for 20 min. The supernatant was collected and gives the PANI-GQD nanocomposite. The synthesis of pure PANI is similar to the above procedure except the GQD solution was replaced with DI water and without subsequent centrifugation.

Fabrication of devices

15 Interdigitated electrodes consisting of 20 fingers, each separated at 25 µm and having a width of 30 µm were fabricated on 300 nm SiO₂/Si substrate by standard photolithography technique. Ti/Au (10/100 nm) electrodes were deposited by magnetron sputtering. Substrates with pre-patterned electrodes were cleaned with acetone, isopropanol, DI water and oxygen plasma, then 100 µl of pure GQD or PANI-GQD solution was dropped onto the electrodes and spin-coated at 2000 rpm for 30 s. The devices were first dried in ambient condition for one day before heated at 90 °C for 30 min. The GQD and PANI-GQD devices were then 25 used for photoresponse measurements.

Results and Discussion

Characterization of GQD and PANI-GQD

Fig. 1(a) shows the transmission electron microscopy (TEM) image of the GQDs. The GQDs disperse uniformly on the copper grid. No additional surface passivation is required to prevent aggregation of the GQDs. The size of the GQDs ranges from 2 to 7 nm, with an average diameter of 4.58 nm. Fig. 1(b) shows the high-resolution TEM (HR-TEM) image of a GQD. The lattice spacing is measured to be 0.21 nm, which corresponds to the [110] planes of graphite.¹⁹ Fig. 1(c)-(d) show the TEM images of the PANI-GQD. The polymer forms separate island-like matrices

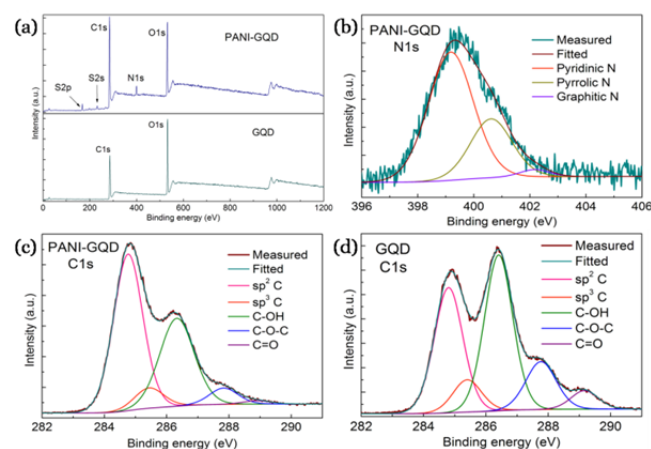


Figure 2 (a) Full scan XPS spectra of PANI-GQD (up) and GQD (down). (b) The N1s XPS spectrum of PANI-GQD. (c) and (d) The C1s spectrum of PANI-GQD and GQD respectively.

as typically shown in Fig. 1(c), with GQDs embedded in it. The GQDs in the nanocomposite have an average diameter of 4.54 nm and again they do not aggregate. The functionalization does not 40 significantly impact the size and shape of the GQDs, as discussed in detail in previous work.²¹

The X-ray photoelectron spectroscopy (XPS) spectra of the GQDs and PANI-GQD are shown in Fig. 2. The PANI-GQD has additional peaks of N and S, apart from the C and O peaks 45 observed in the GQD, which are originated from PANI. The C1s peaks are deconvoluted into five peaks located at 284.8 eV (sp² carbon), 285.4 eV (sp³ carbon), 286.3 eV (C-OH), 287.8 eV (C-O-C) and 288.9 eV (C=O). It is noticed that the sp² peak of the PANI-GQD is more intense than the GQD, which may be 50 resulted from the extended π -conjugation network from the PANI. The N1s spectrum of the PANI-GQD is composed of three peaks located at 399.2 eV (pyridinic N), 400.6 eV (pyrrolic N) and 402.2 eV (graphitic N), where pyridinic N is the dominant component.

55 The effect of functionalization of the GQDs with PANI is clearly observed from the ultraviolet-visible (UV-Vis) spectrum as shown in Fig. 3(a). The GQDs exhibit two absorption peaks at ca. 228 nm and 284 nm, which corresponds to the π to π^* transition of C-C and n to π^* transition of C=O bond respectively.²² The 60 PANI-GQD also exhibit the above two peaks but have one additional peak at ca. 365 nm. The appearance of the new absorption peak after functionalization often indicates the formation of charge transfer complex.²³⁻²⁴ Aniline consists of an amine group, which is bonded to the GQD after 65 functionalization.²¹ The unpaired electron in the amine group facilitates electron donation to the GQD.¹⁶ In the inset of Fig. 3(b), it can be seen that this new peak red-shifts from 357 to 388 nm when increasing the amount of aniline added in the synthesis. This indicates that the origin of the new peak is closely related to 70 the functionalization. In addition, the intensity of the peak at ca. 284 nm due to the C=O bond decreases continuously with increasing amount of aniline. It is expected that the number of aromatic amine group on the GQDs would increase¹³ as more aniline is added and replace the oxygen functional groups on the 75 GQD surface.

The Fourier transform infra-red (FTIR) spectra of the PANI,

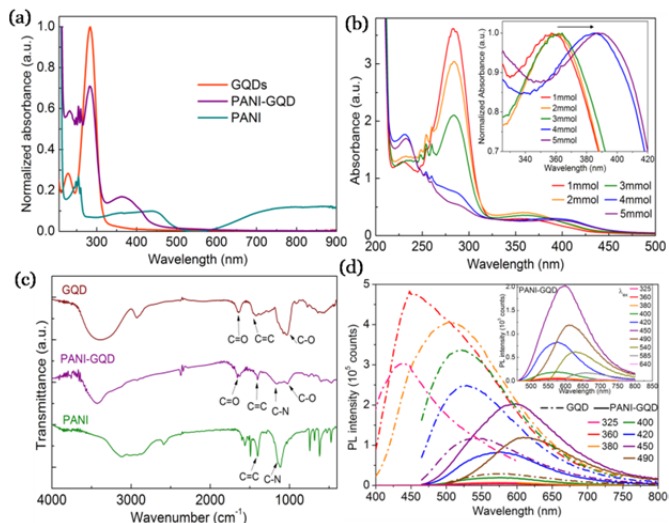


Figure 3 (a) The UV-Vis absorption spectra of the GQDs, PANI-GQD and PANI. (b) The UV-Vis spectra of PANI-GQD prepared with 1 to 5 mmol of aniline monomer. Inset: red-shift of the absorption peak at ca. 375 nm with increasing amount of aniline. (c) FTIR spectra of the GQD, PANI-GQD and PANI. (d) PL spectra of the GQD and PANI-GQD for different excitation wavelengths. Inset is the magnified PL spectra of the PANI-GQD.

GQDs and PANI-GQD are shown in Fig. 3(c). Absorption peaks at ca. 1020 and 1160 cm^{-1} correspond to the C-O and C-N bonds respectively. The peaks at ca. 1400-1450 and 1650 cm^{-1} corresponds to the C=C and C=O bonds respectively. The PANI-GQD expresses the features of both GQDs and PANI. The C=O peak is observed in the PANI-GQD and GQDs but not PANI, due to the absence of carbonyl group in PANI. In addition, the GQDs have a broad peak at ca. 1000-1450 cm^{-1} due to the abundant in C-O bond from carboxyl and hydroxyl groups in pure GQDs, while PANI-GQD and PANI exhibit a sharp peak resulted from the C=C bond. This is also evident from the C1s XPS spectra where the C=O, C-O-C and C-OH peaks are diminished in the PANI-GQD as compared to the GQDs.

To perform the photoluminescence (PL) measurements, equal volume (600 μl) of the GQD or PANI-GQD solution is transferred to quartz cuvettes without dilution. Under the same excitation wavelength (λ_{ex}), the PL peak of the PANI-GQD shows a red shift from that of the GQDs as shown in Fig. 3(d). The red shift is persistent for λ_{ex} ranges from 325 to 640 nm. Red shift of PL peak when compared with the GQDs is also reported for GQDs functionalized with NH_3^{13} and PEG-diamine¹⁶, and is attributed to electron transfer from amine group to GQD which narrows the band gap. As described above, the amine group present in aniline also induces similar charge transfer and causes the PL tuning property in PANI-GQD.

From Fig. 3(d), the maximum PL intensity of the GQDs occurs at ca. 450 nm at $\lambda_{\text{ex}} = 360$ nm while that of the PANI-GQD occurs at ca. 600 nm at $\lambda_{\text{ex}} = 450$ nm. The PANI-GQD exhibits stronger PL than GQD for λ_{ex} longer than 450 nm with the corresponding emission wavelength longer than 600 nm. In other words, PANI-GQD exhibit stronger PL than GQDs when excited by most part of the visible light. This property is advantageous for bio-imaging application, since intense excitation in ultraviolet and blue end of visible region may induce damages to bio-species.^{15, 25}

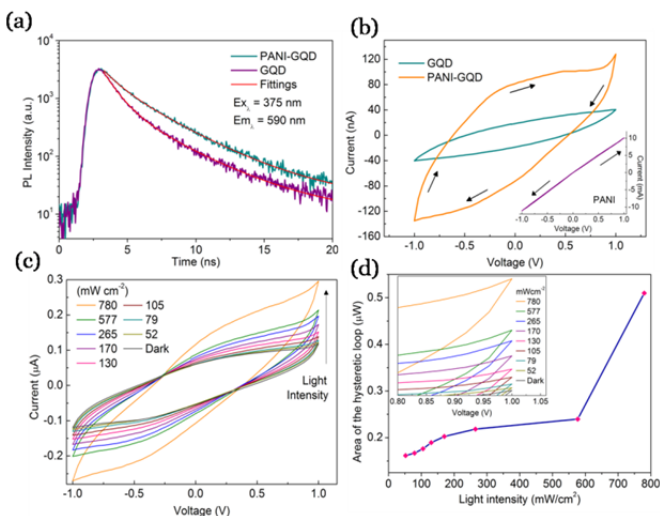


Figure 4 (a) The time-resolved PL decay measurements of the PANI-GQD and GQD with an excitation at 375 nm and emission at 590 nm. The fittings are tri-exponential function. (b) Dark I-V measurements of the GQD and PANI-GQD. Inset: Linear I-V curve of the PANI. (c) I-V curves of the PANI-GQD at different light intensities. (d) Area of the hysteretic loop of the light modulated I-V of the PANI-GQD shown in (c) as a function of light intensity. Inset is the magnified curve of (c) showing the variation of photocurrent.

Fig. 4(a) shows the time-resolved PL spectra of the GQD and PANI-GQD. The PANI-GQD has a longer PL decay time than the GQDs at λ_{ex} of 375 nm. The average decay lifetime for the PANI-GQD and the GQDs are 3.98 and 3.51 ns respectively. PL of the GQD originates from intrinsic state emission due to quantum confinement and defect state emission.⁹ The increase in decay lifetime of the composite can be related to the change in surface states which alter the defect state emission. Raman spectrum of the PANI-GQD, thermogravimetric analysis (TGA), the shift of PL peaks of the PANI-GQD with the amount of aniline and excitation dependent PL of the PANI-GQD are provided in Supporting Information (SI) Fig. S1 –S4 respectively.

Photoresponse measurements

Electrical measurements were carried out with Keithley 2400 sourcemeter in the ambient condition. The *I-V* measurement performed in the dark for the GQD and PANI-GQD devices are shown in Fig. 4(b). The GQD and PANI-GQD exhibit persistent hysteretic *I-V* in all 20 sweeping cycles. Hysteretic *I-V* implies the existence of multiple resistance states which has been exploited in resistive memory devices.^{17–18} When voltage sweeps from positive to negative direction, a high resistance state is obtained, and the opposite sweeping direction gives a low resistance state. However, *I-V* measurement on PANI does not show hysteresis as shown in the inset in Fig. 4(b). Hysteretic *I-V* curve had been reported in separate works for GQD, P3HT-GQD and PEG-GQD composite films^{17–18, 26}, but the hysteretic behaviour of the GQD and composite had not been compared. Therefore the effect induced by functionalization is still unclear. Under the same voltage scan range, the PANI-GQD exhibits a larger hysteresis, thus larger energy storage and memory effect, than the GQD as shown in Fig. 4(b). The energy stored is estimated by the area enclosed in the hysteretic loop^{21, 27}, which are calculated to be 9.09 nW and 201.6 nW for GQD and PANI-

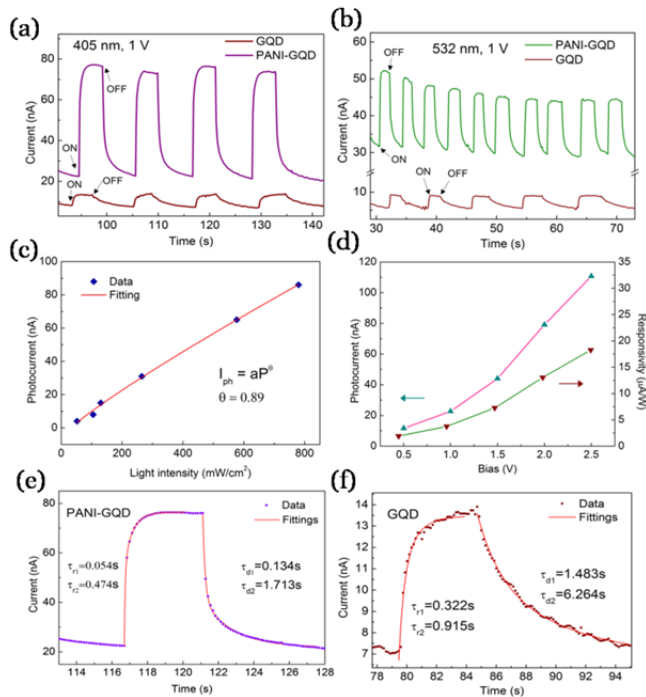


Figure 5 Photoresponse of the PANI-GQD and GQD devices at 1 V at same light intensity under (a) 405 nm and (b) 532 nm illumination. (c) Relationship of the photocurrent with light intensity of the PANI-GQD device. (d) Photocurrent and responsivity at different bias voltages of the PANI-GQD device. (e) Rise and decay time constants obtained from fitting with bi-exponential function of the PANI-GQD (left) and GQD (right) photoresponse.

GQD respectively in the scan range of ± 1 V. It indicates more than one order of magnitude increase in the stored energy in PANI-GQD. Energy stored at different voltage scan ranges are given in SI, Fig. S5.

Apart from tuning the hysteresis of PANI-GQD with the amount of aniline²¹, the hysteresis is also optically tunable as demonstrated in Fig. 4(c). The degree of hysteresis increases with light intensity at a fixed scan range of ± 1 V as illustrated in Fig. 4(d). The stored energy can be increased by three folds upon increasing the light intensity from 52 to 780 mW/cm².

In view of the large difference in PL, light absorption and electrical properties between the GQD and PANI-GQD, their optoelectronic properties are further studied. Photoresponse of the GQD and PANI-GQD are compared by fabricating devices as described in the experimental section. Light sources include a 405 nm and 532 nm laser diodes. Light intensities were measured with a calibrated power meter. The photoresponse of the devices under 405 nm and 532 nm illuminations are shown in Fig. 5(a) and 5(b) respectively. The dark current of the PANI-GQD device is higher than the GQD device. At both wavelengths, the PANI-GQD demonstrates a larger photocurrent than the GQD device under the same light intensity and bias voltage. Responsivity (R) is given by $R = I_{ph}/P$, where I_{ph} is the photocurrent and P is the incident optical power. The responsivity of the PANI-GQD is an order of magnitude higher than that of the GQD at 405 nm, and is 7 folds higher at 532 nm.

Response time, another important parameter for photodetection, of the GQD and PANI-GQD are analyzed in Fig. 5 (e) and 5(f).

The rise and decay time constants are obtained by fitting the temporal response with $I(t) = I_{dark} + A_1 \exp(-t/\tau_{r1}) + A_2 \exp(t/\tau_{r2})$ for growth and $I(t) = I_{dark} + A_1 \exp(-t/\tau_{d1}) + A_2 \exp(-t/\tau_{d2})$ for decay, where $\tau_{r1,2}$ and $\tau_{d1,2}$ are the rise and decay time constants respectively. The rise time of the PANI-GQD device at 405 nm and 1 V bias is two folds faster than the GQD device and the decay time is four folds faster. A summary of the photoresponse parameters of the GQD and PANI-GQD devices is provided in Table 1.

The improved responsivity and response time of the PANI-GQD are attributed to the enhanced inter-connection between the GQDs by the polymer. As revealed in the TEM images, pure GQDs are isolated from each other due to electrical repulsion of the surface functional groups which makes GQD self-passivated. On the other hand, the GQDs are embedded in nano-sized, island-like polymer matrices in the nanocomposite. The polymer facilitates charge transport within the polymer matrices which causes the photoresponse to improve significantly.

The relationship of photocurrent and light intensity of the PANI-GQD device is shown in Fig. 5(c), which is fitted by the power law $I_{ph} = aW^\theta$, where I_{ph} is the photocurrent, and W is the light intensity. The value of θ is 0.89. Fig. 5(d) illustrates the magnitude of photocurrent and responsivity of the PANI-GQD device at different voltages under 405 nm illumination. The responsivity is shown to raise by six folds upon increasing the bias from 0.5 V to 2.5 V.

As the bias voltage increases from 0.5 V to 3 V, the PANI-GQD device exhibits a positive photocurrent upon illumination as shown in Fig. 6(a). Surprisingly, as the bias increases to 4 V, a negative photocurrent is observed as shown in Fig. 6(b), where the light intensity is kept constant in all the measurements. In Fig. 6(b), when the light is on, the current first exhibits a sharp increase, in about 0.5 s, it decreases continuously until a negative photocurrent is achieved. The current increases when the light is off. Negative photocurrent is persistent for a bias larger than 4 V as shown in Fig. 6(b). At 1 V bias, the positive photocurrent does not switch to negative for a prolonged illumination period of over 240 s as shown in SI, Fig. S6. The negative photocurrent can be reverted to positive when the bias is reduced back to below 3 V. This photocurrent switching phenomenon has not been reported for GQD-based optoelectronic devices. In addition, this phenomenon is found largely related to the GQD but not the functionalization, since similar photocurrent switching is also observed in pure GQD devices as shown in Fig. 6(c). Previous work based on photoconductive film of metal nanoparticles coated with charged ligands²⁸ reported a positive photocurrent at 1.6 V which switches to a negative photocurrent at 4 V bias. It is reported that the original neutrally charged

Table 1 Summary of the photoresponse at 1 V of PANI-GQD and GQD devices

Device	I_{ph} at 405 nm (nA)	R at 405 nm ($\mu\text{A}/\text{W}$)	I_{ph} at 532 nm (nA)	R at 532 nm ($\mu\text{A}/\text{W}$)	τ_{r1}/τ_{r2} (s)	τ_{d1}/τ_{d2} (s)
PANI-GQD	52.66	8.69	23.00	1.05	0.054/0.47	0.13/1.71
GQD	5.06	0.835	3.41	0.155	0.32/0.92	1.48/6.26

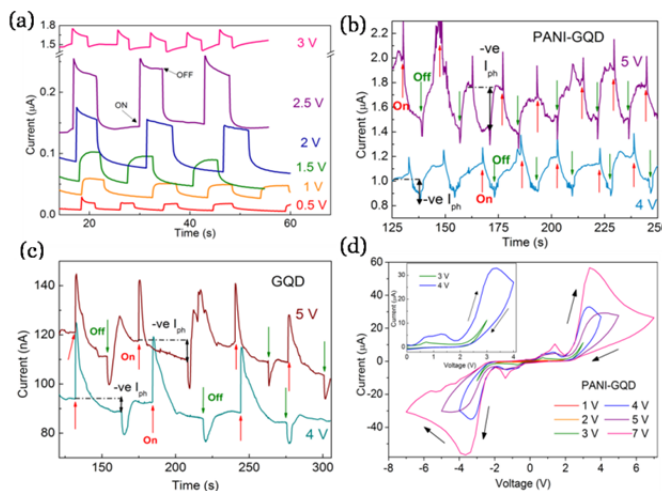


Figure 6 (a) Positive photocurrent of the PANI-GQD device at the bias voltage from 0.5 to 3 V. (b) Negative photocurrent of the PANI-GQD device at 4 and 5 V. (c) Negative photocurrent of the GQD device at 4 and 5 V. (d) I - V characteristics of the PANI-GQD for scan ranges from ± 1 to ± 7 V. Inset shows the I - V curves for scan ranges of 3 and 4 V.

ligands is transformed to charged ligands at higher voltage which has been reported in another work²⁹ to occur at ca. 2 V. A lower charge trapping energy level exists in the charged ligands as compared to the neutrally charged ligands such that photogenerated electrons can be excited to this new trapping energy level and results in negative photocurrent. Another work reported the switch of photocurrent from negative to positive, which is in contrast to this work, on photodetectors with Ag nanoparticles embedded below graphene, as the bias increases from 10 mV to 1 V.³⁰ It is attributed to photo-induced together with plasmonic enhanced electric field induced desorption of charge trapping adsorbates in the air, but no experimental evidence is provided.

The GQDs have large surface-to-volume ratio, with various polar functional groups on the surface as revealed by FTIR and XPS. Polar molecules in the atmosphere would therefore interact strongly with the GQD and interfere with the carrier transport in GQD devices. As a consequence, photocurrent measurements were also conducted in N_2 environment in order to investigate the effect of polar adsorbates on the devices. The devices were heated in N_2 at 90 °C for 30 min to drive away the adsorbates. The current of the PANI-GQD device decreases by several orders of magnitude in N_2 . No regular I - V curve and photoresponse could be recorded as given in Fig. S7. After the device is transferred from N_2 back to the air, photoresponse is observed. It has been similarly reported in Ref. 26 that the conductivity of GQD decreases by 3 orders of magnitude when transferred from air to non-polar gas environment. The role of polar adsorbates in the switching phenomenon remains unclear, but they are shown to have tremendous effect on the electrical transport of GQDs.

At around 4 V, charge carriers are excited into the trapping energy level of the GQD and PANI-GQD. The various voltage scan ranges of the PANI-GQD are shown in Fig. 6(d). For the voltage scan range of ± 4 , ± 5 and ± 7 V, a large drop in current is observed at an onset voltage of about 3.3 V, and continues to drop with increasing voltage. This indicates the onset of significant charge trapping between 3 and 4 V, which is

consistent with our photocurrent measurements. Under photoexcitation, carriers are injected into the trapping energy level. These trapped charges interact with free carriers injected from the electrodes, and results in a net decrease in free charge carriers, and a negative photocurrent is observed.

The origin of the change in charge trapping scenario in the GQD device at higher bias, which could be due to the change from neutral to charged surface functional groups at higher bias²⁸, and interactions with adsorbates in the air³⁰, would require further investigations.

Conclusion

In conclusion, the PANI-GQD devices demonstrate an improved photoresponse as compared with the pristine GQD device. The improved photoresponse is attributed to the enhanced carrier transport as a result of better interconnection of GQD by the island-like polymer matrices. The photocurrent of the GQD and PANI-GQD devices change from positive to negative when the applied voltage is larger than 3 V. Trapping of charge carriers become very significant at high bias voltage and results in net decrease of free charge carriers. The optical switching phenomenon may open up novel applications for GQDs in optoelectronics.

Acknowledgements

The authors thank Dr. Zhike Liu and Dr Wei Lu for the measurements in N_2 environment and TEM characterization respectively. This work was financially supported by the Research Grants Council of Hong Kong (Project Nos. PolyU 5006/12P and PolyU 153012/14P), PolyU grants (Project Nos. G-YN10 and 1-ZE14) and National Natural Science Foundation of China (Grant no. 11374250).

Notes and references

^aDepartment of Applied Physics, The Hong Kong Polytechnic University, 70 Hung Hom, Kowloon, HKSAR.
^bThe Hong Kong Polytechnic University Shenzhen Research Institute, Shenzhen 518057, China.
E-mail: apspalu@polyu.edu.hk

^cMultidisciplinary Nanotechnology Centre, College of Engineering,

Swansea University, Singleton Park, Swansea SA2 8PP, UK

[†]Electronic Supplementary Information (ESI) available: [Raman spectrum of PANI-GQD, TGA, Red-shift of PL peak with the amounts of aniline, excitation dependent PL of PANI-GQD, area of hysteretic loop for different voltage scan ranges, photocurrent at 1 V under prolonged illumination] See DOI: 10.1039/b000000x/

- 1 M. Hassan, E. Haque, K. R. Reddy, A.I. Minett, J. Chen and V. Gomes, *Nanoscale*, 2014, **6**, 11988-11994
- 2 X. Li, S. P. Lau, L. Tang, R. Ji and P. Yang, *J. Mater. Chem. C*, 2013, **1**, 7308-7313
- 3 Y. Zhang, C. Wu, X. Zhou, X. Wu, Y. Yang, H. Wu, S. Guo and J. Zhang, *Nanoscale*, 2013, **5**, 1816-1819
- 4 X. Wu, F. Tian, W. Wang, J. Chen, M. Wu and J. X. Zhao, *J. Mater. Chem. C*, 2013, **1**, 4676-4684
- 5 L. Li, G. Wu, G. Yang, J. Peng, J. Zhao and J. Zhu, *Nanoscale*, 2013, **5**, 4015-4039
- 6 D. I. Son, B. W. Kwon, D. H. Park, W. S. Seo, Y. Yi, B. Angadi, C. L. Lee and W. K. Choi, *Nat. Nanotechnol.*, 2012, **7**, 465-471
- 7 D. H. Wang, J. K. Kim, S. J. Kim, B. H. Hong and J. H. Park, *Nanoscale*, 2014, **6**, 15175-15180

- 8 V. Gupta, N. Chaudhary, R. Srivastava, G. D. Sharma, R. Bhardwaj and S. Chand, *J. Am. Chem. Soc.*, 2011, **133**, 9960-9963
- 9 Z. Huang, Y. Shen, Y. Li, W. Zheng, Y. Xue, C. Qin, B. Zhangm J. Hao and W. Feng, *Nanoscale*, 2014, **6**, 13043-13052
- 10 S. H. Song, M. H. Jang, J. Chung, S. H. Jin, B. H. Kim, S. H. Hur, S. Yoo, Y. H. Cho and S. Jeon, *Adv. Optical Mater.*, 2014, **2**, 1016-1023
- 11 L. Tang, R. Ji, X. Li, G. Bai, C. P. Liu, J. Hao, J. Lin, H. Jiang, K. S. Teng, Z. Yang and S. P. Lau, *ACS Nano*, 2014, **8**, 6312-6320
- 12 J. Shen, Y. Zhu, X. Yang, J. Zong, J. Zhang and C. Li, *New J. Chem.*, 2012, **36**, 97-101
- 13 H. Tetsuka, R. Asahi, A. Nagoya, K. Okamoto, I. Tajima, R. Ohta and A. Okamoto, *Adv. Mater.*, 2012, **24**, 5333-5338
- 14 F. Jiang, D. Chen, R. Li, Y. Wang, G. Zhang, S. Li, J. Zheng, N. Huang, Y. Gu, C. Wang and C. Shu, *Nanoscale*, 2013, **5**, 1137-1142
- 15 S. Zhu, J. Zhang, S. Tang, C. Qiao, L. Wang, H. Wang, X. Liu, B. Li, Y. Li, W. Yu, X. Wang, H. Sun and B. Yang, *Adv. Funct. Mater.*, 2012, **22**, 4732-4740
- 16 S. H. Jin, D. H. Kim, G. H. Jun, S. H. Hong and S. Jeon, *ACS Nano*, 2013, **7**, 1239-1245
- 17 A. C. Obreja, D. Cristea, I. Mihalache, A. Radoi, R. Gavrila, F. Comanescu and C. Kusko, *Appl. Phys. Lett.*, 2014, **105**, 083303
- 18 I. Mihalache, A. Radoi, C. Munteanu, M. Kusko and C. Kusko, *Org. Electron.*, 2014, **15**, 216-225
- 19 L. Tang, R. Ji, X. Li, K. S. Teng and S. P. Lau, *Part. Part. Syst. Charact.*, 2013, **30**, 523-531
- 20 C. M. Luk, L. B. Tang, W. F. Zhang, S. F. Yu, K. S. Teng and S. P. Lau, *J. Mater. Chem.*, 2012, **22**, 22378-22381
- 21 C. M. Luk, B. L. Chen, K. S. Teng, L. Tang and S. P. Lau, *J. Mater. Chem. C*, 2014, **2**, 4526-4532
- 22 S. K. Lai, L. Tang, Y. Y. Hui, C. M. Luk and S. P. Lau, *J. Mater. Chem. C*, 2014, **2**, 6971-6977
- 23 Y. Sun, S. R. Wilson and D. I. Schuster, *J. Am. Chem. Soc.*, 2001, **123**, 5348-5349
- 24 X. Li, B. Wu, J. Huang, J. Zhang, Z. Liu, H. Li, *Carbon*, 2003, **41**, 1670-1673
- 25 B. E. Cohen, *Nature*, 2010, **467**, 407-408
- 26 H. Kalita, V. Harikrishnan, D. B. Shinde, V. K. Pillai and V. K. Pillai, *Appl. Phys. Lett.*, 2013, **102**, 143104
- 27 B. Biswas, A. Chowdhury, M. K. Sanyal, M. Majumder and B. Mallik, *J. Mater. Chem. C*, 2013, **1**, 1211-1222
- 28 H. Nakanishi, K. J. M. Bishop, B. Kowalczyk, A. Nitzan, E. A. Weiss, K. V. Tretiakov, M. M. Apodaca, R. Klajn, J. F. Stoddart and B. A. Grzybowski, *Nature*, 2009, **460**, 371-375
- 29 T. D. Nguyen, H. R. Tseng, P. C. Celestre, A. H. Flood, Y. Liu, J. F. Stoddart and J. I. Zink, *Proc. Natl. Acad. Sci. U.S.A.*, 2005, **102**, 10029-10034
- 30 C. Y. Liu, K. Liang, C. C. Chang and Y. Tzeng, *Opt. Express.*, 2012, **20**, 22943-22952